Real-Space Coexistence of the Melted Mott State and Superconductivity in Fe-Substituted 1T-TaS_2

R. Ang,[1] Y. Tanaka,[2] E. Ieki,[2] K. Nakayama,[2] T. Sato,[2] L. J. Li,[3] W. J. Lu,[3] Y. P. Sun,[3,4] and T. Takahashi[1,2]

[1]*WPI Research Center, Advanced Institute for Materials Research, Tohoku University, Sendai 980-8577, Japan*

[2]*Department of Physics, Tohoku University, Sendai 980-8578, Japan*

[3]*Key Laboratory of Materials Physics, Institute of Solid State Physics, Chinese Academy of Sciences, Hefei 230031, China*

[4]*High Magnetic Field Laboratory, Chinese Academy of Sciences, Hefei 230031, China*

(Received 14 July 2012; published 23 October 2012)

We have performed high-resolution angle-resolved photoemission spectroscopy of layered chalcogenide 1T-$Fe_xTa_{1-x}S_2$ which undergoes a superconducting transition in the nearly commensurate charge-density-wave phase (melted Mott phase). We found a single electron pocket at the Brillouin-zone center in the melted Mott phase, which is created by the backfolding of bands due to the superlattice potential of charge-density-wave. This electron pocket appears in the x region where the samples show superconductivity, and is destroyed by the Mott- and Anderson-gap opening. Present results suggest that the melted Mott state and the superconductivity coexist in real space, providing a new insight into the interplay between electron correlation, charge order, and superconductivity.

DOI: 10.1103/PhysRevLett.109.176403 PACS numbers: 71.45.Lr, 71.20.−b, 71.30.+h, 79.60.−i

Cooperation or competition of superconductivity with various orders like charge order or charge-density-wave (CDW) is a long-standing, yet unestablished issue in low-dimensional physics. Conventional CDW order is well explained by the nesting of the Fermi surface (FS) driven by electron-phonon coupling, resulting in new charge periodicity accompanied by the lattice distortion. While this Peierls mechanism explains the fundamental aspect of the CDW characteristics in various systems, electron correlation also plays an important role in some of the low-dimensional materials, leading to multiple ordered phases in the proximity of the charge-ordered phase, which may be a prerequisite of unconventional physical properties, as highlighted by the complex phase diagram in organic salts [1], high-temperature superconducting (SC) cuprates [2,3], and heavy fermions [4].

Layered transition-metal dichalcogenides (TMDs) provide an ideal platform for investigating the interplay between electron correlation, CDW, superconductivity, and other electronic orders, essentially owing to their quasi-two-dimensional (2D) crystal structure being susceptible to various electronic instabilities [5,6]. Among many TMD materials, 1T-TaS_2 has received special attention since it exhibits a Mott insulating phase besides the CDW formation due to the strong electron-phonon and electron-electron interactions [7–11]. As shown in Fig. 1(a), the phase diagram of pristine 1T-TaS_2 is characterized by a high-temperature normal metallic phase, followed by a nearly commensurate CDW (NCCDW) phase and commensurate CDW (CCDW) phase coexisting with a Mott insulating phase.

The Mott insulating phase of 1T-TaS_2 is quite unique. Ta atoms are displaced to form star-of-David clusters where twelve Ta atoms contract toward a central atom, and each cluster is interlocked by forming a triangular superlattice with a $\sqrt{13} \times \sqrt{13}$ periodicity [7,8,12], accompanied by the narrowing of the Ta 5d valence band and the formation of multiple subbands due to band folding [13,14]. Upon increasing temperature, the Mott phase melts into the NCCDW phase (the melted Mott phase) with a sudden resistivity drop, where several tens of stars organize into roughly hexagonal domains [15], locally reproducing the CCDW Mott phase. Time-resolved photoemission and diffraction experiments suggest extremely fast charge responses across the melting of the Mott phase [16–20], implying that the mechanism of CCDW is beyond the conventional Peierls picture.

Distinct from other 1T-type TMDs, superconductivity emerges in 1T-TaS_2 by applying high pressure [21] or introducing disorders in the crystal [22]. It has been reported recently [23] that substitution of Ta with Fe in 1T-TaS_2 induces superconductivity in the NCCDW state, spanned by the Mott-insulating and Anderson localization (AL) phases [Fig. 1(a)]. A rich electronic phase diagram of this material provides a precious opportunity to study the interplay (i.e., coexistence, competition, and collaboration) among various ground states. However, such an investigation has not yet been made, owing essentially to the fact that it is hard to reach the SC and AL phases in pristine 1T-TaS_2 at ambient conditions.

In this Letter, we report high-resolution angle-resolved photoemission spectroscopy (ARPES) of 1T-$Fe_xTa_{1-x}S_2$. We directly accessed the above essential issue by elucidating the electronic states of all the available electronic phases. Our results suggest that the superconductivity is characterized by a shallow electron pocket at the Brillouin-zone center, and the SC and melted Mott states coexist in the real space.

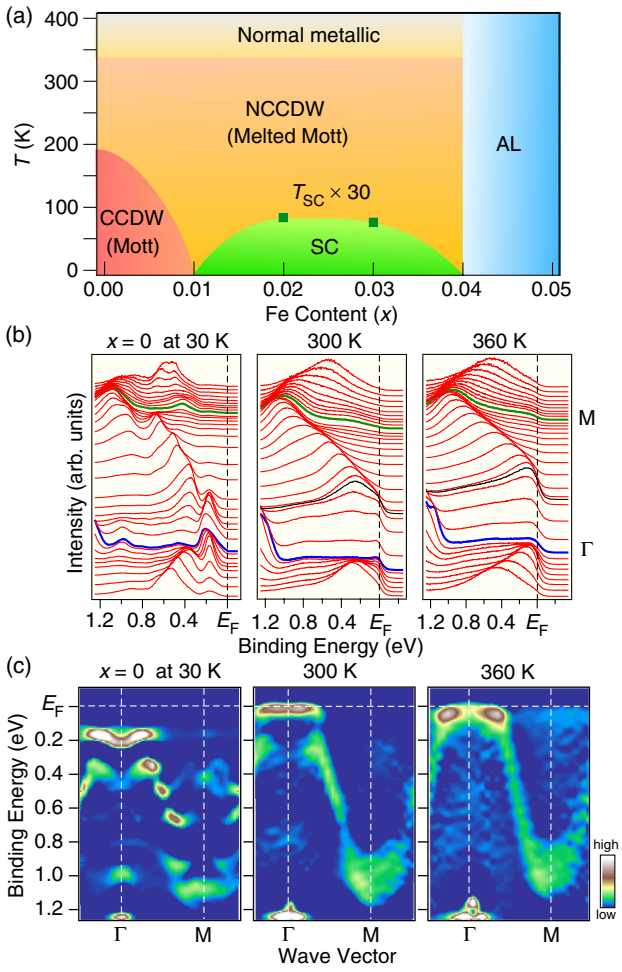

FIG. 1 (color online). (a) Schematic electronic phase diagram of $1T$-$Fe_xTa_{1-x}S_2$ derived from transport properties [23] as a function of temperature and x, where CCDW, NCCDW, SC, and AL represents the commensurate CDW, nearly commensurate CDW, superconductivity, and Anderson localization, respectively. For $x = 0.02$ and 0.03, the SC critical temperature T_c is 2.8 and 2.6 K, respectively. (b) EDCs of pristine $1T$-TaS_2 measured at 30, 300, and 360 K along the ΓM direction. (c) Corresponding second-derivative ARPES intensity $1T$-TaS_2 plotted as a function of wave vector and E_B.

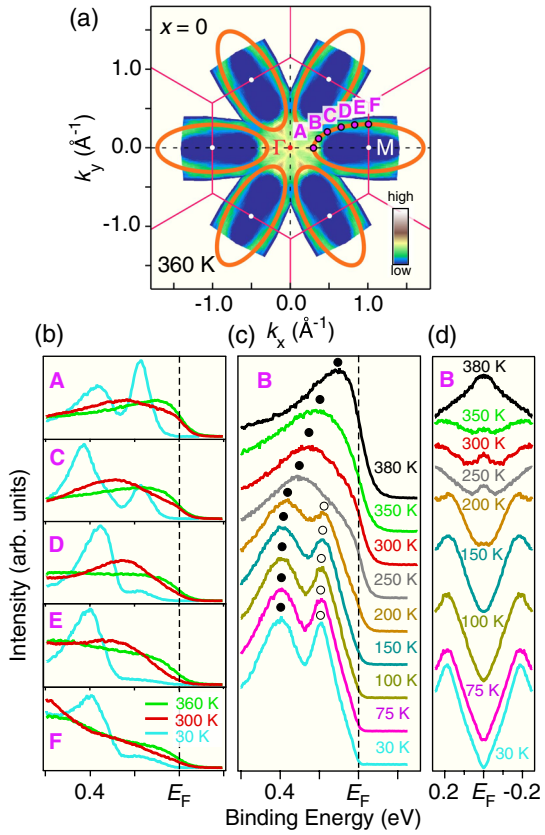

FIG. 2 (color online). (a) 2D ARPES intensity plot of pristine $1T$-TaS_2 measured at $T = 360$ K. Orange circles correspond to the normal-state FS. (b) EDCs at five representative k_F points (A–F) shown in (a), measured at $T = 360$, 300, and 30 K. (c) Temperature dependence of the EDCs at point B. (d) Symmetrized EDCs near E_F.

High-quality single crystals of $1T$-$Fe_xTa_{1-x}S_2$ were grown by the chemical vapor transport method with iodine as a transport agent. Details of the sample preparation were described elsewhere [23]. ARPES measurements were performed using a VG-SCIENTA SES2002 spectrometer with a high-flux He discharge lamp at Tohoku University. The He-$I\alpha$ ($h\nu = 21.218$ eV) resonance line was used to excite photoelectrons. The samples were cleaved *in situ* in an ultrahigh vacuum better than 5×10^{-11} Torr. The energy and angular (k) resolutions were set at 13 meV and 0.2° (0.007 Å^{-1}), respectively. The Fermi level (E_F) of the samples was referenced to that of a gold film evaporated onto the sample holder.

First we focus on the electronic states of pristine $1T$-TaS_2 in which we have revealed some new aspects across the phase transitions. Figures 1(b) and 1(c) show energy distribution curves (EDCs) and corresponding band dispersions of pristine $1T$-TaS_2 along the ΓM cut measured at three different phases [Mott phase (30 K); NCCDW phase (300 K); and normal phase (360 K)]. At $T = 360$ K, we recognize a highly dispersive band around the Γ point. This band crosses E_F at midway between the Γ and M points, forming an electronlike FS centered at the M point [see Fig. 2(a)] [11,13,24]. As shown in Fig. 1(b), this band does not cross E_F at $T = 300$ K but disperses back toward the higher binding energy (E_B) near the k_F (Fermi vector) point in the 360-K spectra (see EDCs marked by a black curve), with a characteristic pseudogap feature [25]. Such band-folding behavior and ARPES-intensity modification are likely caused by the superlattice potential of the NCCDW where the star-of-David clusters locally maintain the $\sqrt{13} \times \sqrt{13}$ periodicity identical to the CCDW Mott phase. Inside the pseudogap, a narrow band pinned at E_F is also observed around the Γ point [see the 300-K intensity in Fig. 1(c)]. In the Mott phase at $T = 30$ K, the Ta $5d$ band splits into multiple subbands due to strong CDW potential. Also, the near-E_F spectral weight resides on the higher E_B side of ~0.2 eV due to the Mott-Hubbard gap opening,

which is triggered by the narrow bandwidth of the flat band at E_F and resultant enhancement of an effective electron correlation [9,13,16,20]. It is emphasized here that, while previous ARPES studies rather focused on the Mott transition [22,25–27], the present ARPES result clearly establishes that there is also a distinct change in the electronic states across the NCCDW transition at high temperature.

To see the evolution of electronic states across the Mott and NCCDW transitions, we performed momentum (k)- and temperature-dependent ARPES measurements. Figure 2(b) displays the EDCs measured at various k_F points on the large electron pocket [see Fig. 2(a)]. At $T = 360$ K, the midpoint of the leading edge is located approximately at E_F in the entire k region, indicating the absence of an energy gap. On the other hand, at $T = 300$ K (the NCCDW phase), the spectral weight at E_F is significantly suppressed and transferred to the higher E_B of ~0.3 eV due to the pseudogap opening [24,25]. No signature of the pseudogap at $T = 360$ K demonstrates that the previously identified pseudogap at room temperature [24,25] is of NCCDW origin. As also visible in Fig. 2(b), the spectral weight suffers drastic changes at $T = 30$ K with characteristic peak features at ~0.2 and ~0.4 eV. As seen in Fig. 2(c), the 0.4-eV peak already exists above the Mott phase and evolves below the NCCDW transition temperature, suggesting that it is attributed to the NCCDW gap. On the other hand, the 0.2-eV peak is obviously of Mott-transition origin and is assigned as the lower Hubbard band (LHB) [16,26,27], since it appears at $T = 200$ K close to the Mott-transition temperature. As also visible in Fig. 2(d), a narrow peak appears at E_F in the symmetrized EDCs at 250–350 K. This peak is related to the narrow band formation by the NCCDW transition, and is assigned as a quasiparticle peak (the coherent part of spectral function). This peak completely disappears below 200 K accompanied by a marked reduction of the spectral weight at E_F and the emergence of the LHB (the incoherent part of spectral function). This suggests an abrupt change in the electronic states across the Mott transition, consistent with previous ARPES studies [28,29]. Such an evolution of the spectral feature is qualitatively explained by the dynamical mean-field theory which predicted a similar evolution of the coherent and incoherent spectral weights on varying the effective electron correlation (U/W), supporting the electron-correlation-driven CCDW Mott transition.

Next we turn our attention to the Fe-substitution-induced evolution of electronic states in $1T$-$Fe_xTa_{1-x}S_2$. Figure 3(a) displays the comparison of ARPES intensity plots along the ΓM direction at $T = 350$ K for $x = 0$, 0.02 (normal phase), and 0.05 (AL phase). Obviously, the overall band dispersion for three different Fe concentrations looks quite similar. It commonly shows an electronlike band centered at the M point. In fact, when we extract the peak position of the EDCs for different x values, they match fairly well [see Fig. 3(b)], suggesting that extra carriers provided by the Fe substitution is very small. A closer look at Fig. 3(a) further reveals that the spectral feature is broadened and the near-E_F spectral weight is significantly suppressed only for $x = 0.05$. This is caused by the Fe-induced disorder and resultant AL, consistent with the transport measurement [23]. In fact, when we compare the EDCs at the k_F point, the EDC for $x = 0.0$–0.03 exhibits a Fermi-edge cutoff, while that for $x = 0.04$ and 0.05 shows a broader leading edge with its

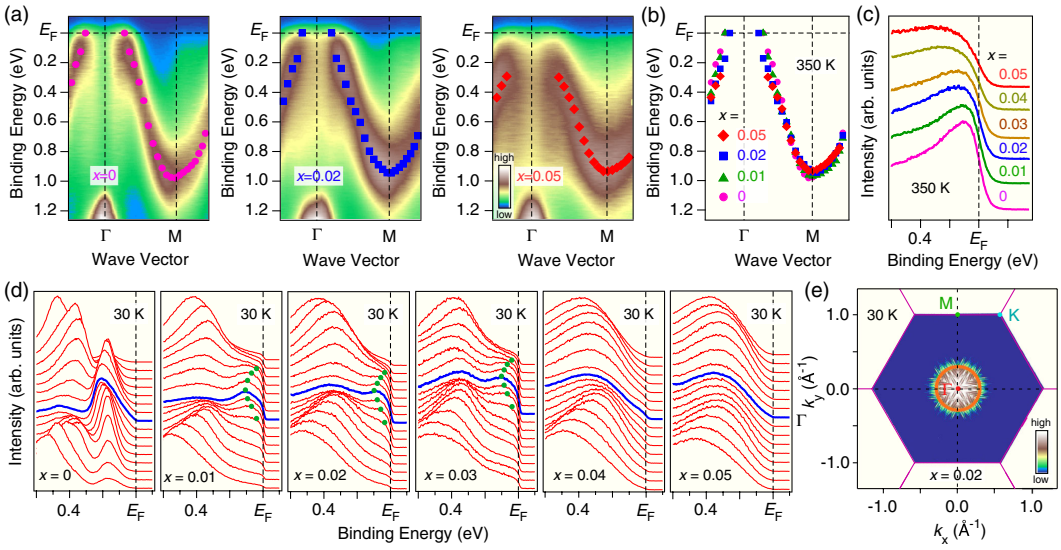

FIG. 3 (color online). (a) ARPES intensity of $1T$-$Fe_xTa_{1-x}S_2$ measured along the ΓM direction for $x = 0$, 0.02, and 0.05, plotted as a function of wave vector and E_B in the normal metallic phase ($T = 350$ K). (b) Direct comparison of the band dispersions for $x = 0$, 0.01, 0.02, and 0.05 at $T = 350$ K. The energy positions of the bands are determined by tracing the peak position of EDCs. (c) Comparison of ARPES spectra at the k_F point along the ΓM direction. (d) x dependence of EDCs around the Γ point in $1T$-$Fe_xTa_{1-x}S_2$ at $T = 30$ K. (e) ARPES intensity plot as a function of a 2D wave vector for $x = 0.02$. Intensity is obtained by assuming the hexagonal symmetry.

midpoint located at a higher E_B, a hallmark of the AL as reported in other AL systems [30,31].

A most important finding is presented in Fig. 3(d), which plots the Fe-concentration dependence of EDCs around the Γ point at $T = 30$ K covering the Mott phase ($x = 0$), the NCCDW phase ($x = 0.01$–0.03), and the AL phase ($x = 0.04$ and 0.05). Evidently, there exists a shallow electron pocket centered at the Γ point whose bottom is $\sim$0.1 eV below E_F. Since this electron pocket is not observed in the normal phase [see Fig. 3(a)] nor in the Mott or AL phase, it is characteristic of the NCCDW phase, and likely created by the backfolding of bands due to the superlattice potential of NCCDW. This is also supported by the band calculations with a superlattice potential [11,24] which predicted a similar electron pocket at the Γ point. We have surveyed the electronic states near E_F in the NCCDW phase and found that the strong ARPES intensity is seen only around the Γ point in the NCCDW phase, as highlighted in Fig. 3(e). This suggests that the large electron pocket at the M point observed in the normal phase is essentially gapped in the entire k region in the NCCDW phase, and the shallow electron pocket at the Γ point dominates the transport properties in the NCCDW phase. It is thus natural to conclude that the superconductivity is also characterized by the shallow electron pocket at the Brillouin-zone center, since the SC region appears inside the NCCDW phase [see also Fig. 1(a)]. We will discuss implications of this observation later in detail.

The next important issue is the possible link between the emergence of the shallow pocket and the Mott or AL phases. Figure 4(a) displays the x dependence of various energy gaps, compared with that of the density of states (DOS) at E_F of the shallow electron pocket. As immediately noticeable from Fig. 4(a), the Mott or AL gap distinctly has an anti-correlation behavior with the DOS at E_F; when the Mott gap disappears at $x = 0.01$, the DOS enhances, and is the same for the AL gap at $x \sim 0.04$. This strongly suggests that the superconductivity and the Mott and AL states apparently compete with each other. On the other hand, there is no such anti-correlation between the NCCDW gap and the DOS at E_F: the NCCDW gap looks insensitive to Fe substitution while the DOS appears to follow the SC dome shape. We also note that the NCCDW gap does not completely disappear even in the AL phase, probably because of the existence of small NCCDW domains in the AL phase.

Figure 4(b) summarizes the band picture for different electronic phases determined from the present ARPES result. While the normal phase is a weakly correlated metal where the one-electron approach satisfactorily explains the observed band features, a shallow electron pocket appears only in the NCCDW phase and characterizes the transport properties of the NCCDW phase as well as the superconductivity. The pocket is gapped in the Mott phase due to an enhanced electron correlation, and it also smears out by the strong disorders and the resultant Anderson gap opening in the AL phase, both of which are common in the sense that

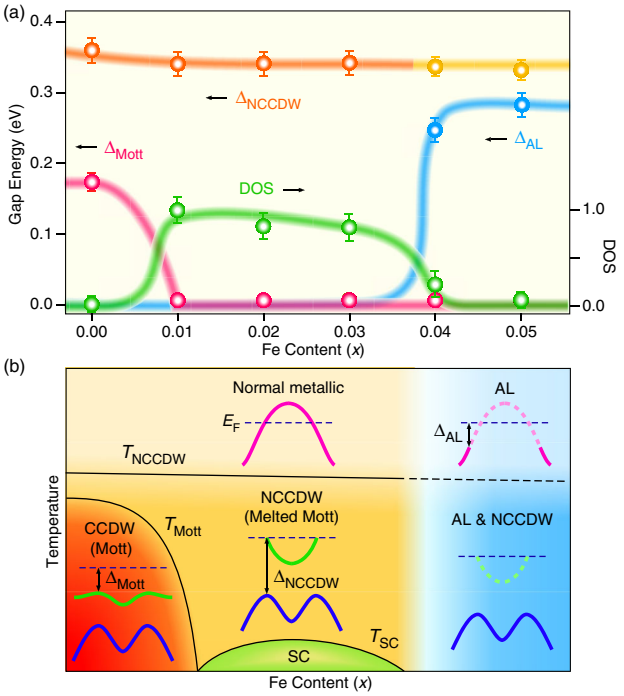

FIG. 4 (color online). (a) Various gap energies (the Mott gap Δ_{Mott}, the NCCDW gap Δ_{NCCDW}, and the AL gap Δ_{AL}) and density of states (DOS) at E_F of an electron pocket plotted as a function of x. The Δ_{Mott} value was estimated by the peak position of the EDC at the minimum-gap k locus of the weakly dispersing lower Hubbard band (LHB), while the Δ_{NCCDW} and Δ_{AL} values were determined by the EDC peak position at the k_F point along the ΓM direction in the normal phase (note that the gap value does not strongly depend on the particular selection of the k_F point because of its nearly isotropic nature). The DOS at E_F is estimated by the intensity at E_F of EDCs integrated along the ΓM direction, normalized to the 0.4-eV peak. (b) Schematic band diagram derived from the present ARPES experiment as a function of temperature and x. Dashed curve represents the absence of the band.

they remove the mobile carriers responsible for the superconductivity. Such a fragile nature of the pocket against localization implies the competing nature of the superconductivity with Mott and Anderson localizations.

Now we discuss the implications of a shallow electron pocket in the NCCDW phase. We infer that the superconductivity is likely characterized by this electron pocket, by considering (i) its dominant intensity contribution in the k space in the NCCDW phase, and (ii) the x dependence of the electron-pocket DOS following the SC-dome shape. Based on the experimental fact that the pocket originates from the backfolding of bands due to the superlattice potential of the NCCDW, we reached an unexpected conclusion that the NCCDW and superconductivity coexist in the real space (i.e., within the star-of-David clusters), contrary to the previous conjecture where the superconductivity and the metallic conduction were believed to occur in the interdomain spaces among tens of star-of-David clusters [21]. If the interdomain site is metallic, the E_F crossing of bands should

be observed in the NCCDW phase at the k point where the normal-state FS exists, while our ARPES measurements do not reveal such a band crossing, supporting the real-space coexistence of the NCCDW and the superconductivity. Our finding that the shallow electron pocket also transforms into the LHB in the Mott phase further suggests an intimate link between the electron correlations and the superconductivity in this system.

Finally, we briefly comment on the relationship between the present ARPES experiment and the previous high-pressure experiment of pristine $1T$-TaS_2 [21]. It was reported that the superconductivity of $1T$-TaS_2 extends over a wide pressure range including not only in the NCCDW phase but also in the normal metallic phase. Since it is reasonable to assume that the superconductivity in the normal metallic phase is characterized by the large electron pocket at the M point, it is suggested that the SC characteristics between the NCCDW phase and the normal metallic phase would be different from each other due to the marked difference in the FS topology. In this regard, it would be interesting to investigate the SC properties in the vicinity of the phase boundary between the NCCDW and the normal metallic phase to study possible competition or coexistence between different SC phases.

In summary, we have reported a systematic ARPES study on $1T$-$Fe_xTa_{1-x}S_2$ over a wide x and temperature range. We found direct evidence for the shallow electron pocket at the Γ point in the melted Mott phase, while there is no such FS in the Mott-insulating and AL phases. We have discussed that the electron pocket is created by the backfolding of bands due to the superlattice potential of the NCCDW. We have concluded that the superconductivity and the melted Mott state coexist in the real space. The present results suggest that the $1T$-$Fe_xTa_{1-x}S_2$ is a prime candidate for studying the interplay between electron correlation, CDW, and superconductivity.

This work was supported by grants from JSPS, JST-CREST, MEXT of Japan, and National Key Basic Research of China under Contract No. 2011CBA00111 (Y. P. S., W. J. L., and L. J. L.).

[1] S. Lefebvre, P. Wzietek, S. Brown, C. Bourbonnais, D. Jérome, C. Mézière, M. Fourmigué, and P. Batail, Phys. Rev. Lett. **85**, 5420 (2000).
[2] E. Dagotto, Rev. Mod. Phys. **66**, 763 (1994).
[3] A. Damascelli, Z. Hussain, and Z. X. Shen, Rev. Mod. Phys. **75**, 473 (2003).
[4] N. D. Mathur, F. M. Grosche, S. R. Julian, I. R. Walker, D. M. Freye, R. K. W. Haselwimmer, and G. G. Lonzarich, Nature (London) **394**, 39 (1998).
[5] L. F. Mattheiss, Phys. Rev. B **8**, 3719 (1973).
[6] A. M. Gabovich, A. I. Voitenko, and M. Ausloos, Phys. Rep. **367**, 583 (2002).
[7] J. A. Wilson, F. J. Di Salvo, and S. Mahajan, Adv. Phys. **24**, 117 (1975).
[8] P. Fazekas and E. Tosatti, Philos. Mag. B **39**, 229 (1979); Physica (Amsterdam) **99B+C**, 183 (1980).
[9] R. Manzke, T. Buslaps, B. Pfalzgraf, M. Skibowski, and O. Anderson, Europhys. Lett. **8**, 195 (1989).
[10] R. E. Thomson, B. Burk, A. Zettl, and J. Clarke, Phys. Rev. B **49**, 168 99 (1994).
[11] Th. Pillo, J. Hayoz, H. Berger, R. Fasel, L. Schlapbach, and P. Aebi, Phys. Rev. B **62**, 4277 (2000).
[12] C. B. Scruby, P. M. Williams, and G. S. Parry, Philos. Mag. **31**, 255 (1975).
[13] N. V. Smith, S. D. Kevan, and F. J. DiSalvo, J. Phys. C **18**, 3175 (1985).
[14] K. Rossnagel and N. V. Smith, Phys. Rev. B **73**, 073 106 (2006).
[15] A. Spijkerman, J. L. de Boer, A. Meetsma, G. A. Wiegers, and S. van Smaalen, Phys. Rev. B **56**, 13 757 (1997).
[16] L. Perfetti, P. A. Loukakos, M. Lisowski, U. Bovensiepen, H. Berger, S. Biermann, P. S. Cornaglia, A. Georges, and M. Wolf, Phys. Rev. Lett. **97**, 067 402 (2006).
[17] S. Hellmann *et al.*, Phys. Rev. Lett. **105**, 187 401 (2010).
[18] M. Eichberger, H. Schäfer, M. Krumova, M. Beyer, J. Demsar, H. Berger, G. Moriena, G. Sciaini, and R. J. D. Miller, Nature (London) **468**, 799 (2010).
[19] K. Ishizaka *et al.*, Phys. Rev. B **83**, 081 104 (R) (2011).
[20] J. C. Petersen *et al.*, Phys. Rev. Lett. **107**, 177 402 (2011).
[21] B. Sipos, A. F. Kusmartseva, A. Akrap, H. Berger, L. Forró, and E. Tutiš, Nature Mater. **7**, 960 (2008).
[22] P. Xu, J. O. Piatek, P.-H. Lin, B. Sipos, H. Berger, L. Forró, H. M. Rønnow, and M. Grioni, Phys. Rev. B **81**, 172 503 (2010).
[23] L. J. Li, W. J. Lu, X. D. Zhu, L. S. Ling, Z. Qu, and Y. P. Sun, Europhys. Lett. **97**, 67 005 (2012).
[24] M. Bovet, S. van Smaalen, H. Berger, R. Gaal, L. Forró, L. Schlapbach, and P. Aebi, Phys. Rev. B **67**, 125 105 (2003); M. Bovet, D. Popović, F. Clerc, C. Koitzsch, U. Probst, E. Bucher, H. Berger, D. Naumović, and P. Aebi, *ibid.***69**, 125 117 (2004).
[25] Th. Pillo, J. Hayoz, H. Berger, M. Grioni, L. Schlapbach, and P. Aebi, Phys. Rev. Lett. **83**, 3494 (1999).
[26] F. Zwick, H. Berger, I. Vobornik, G. Margaritondo, L. Forró, C. Beeli, M. Onellion, G. Panaccione, A. Taleb-Ibrahimi, and M. Grioni, Phys. Rev. Lett. **81**, 1058 (1998).
[27] L. Perfetti, T. A. Gloor, F. Mila, H. Berger, and M. Grioni, Phys. Rev. B **71**, 153 101 (2005).
[28] B. Dardel, M. Grioni, D. Malterre, P. Weibel, Y. Baer, and F. Lévy, Phys. Rev. B **46**, 7407 (1992).
[29] F. Clerc, C. Battaglia, M. Bovet, L. Despont, C. Monney, H. Cercellier, M. G. Garnier, P. Aebi, H. Berger, and L. Forró, Phys. Rev. B **74**, 155 114 (2006).
[30] S. Raj, D. Hashimoto, H. Matsui, S. Souma, T. Sato, T. Takahashi, D. D. Sarma, P. Mahadevan, and S. Oishi, Phys. Rev. Lett. **96**, 147 603 (2006).
[31] T. Mizokawa, A. Fujimori, H. Namatame, K. Akeyama, and N. Kosugi, Phys. Rev. B **49**, 7193 (1994).